JACS
JOURNAL OF THE AMERICAN CHEMICAL SOCIETY
Communication
pubs.acs.org/JACS

Single-Layer Single-Crystalline SnSe Nanosheets

Lun Li,[†,‡] Zhong Chen,[†,‡] Ying Hu,[‡] Xuewen Wang,[‡] Ting Zhang,[‡] Wei Chen,[‡] and Qiangbin Wang*[,†,‡]

[†]Division of Nanobiomedicine and [‡]*i*-Lab, Suzhou Institute of Nano-Tech and Nano-Bionics, Chinese Academy of Sciences, Suzhou 215123, P. R. China

Supporting Information

ABSTRACT: Single-layer single-crystalline SnSe nanosheet with four-atomic thickness of ∼1.0 nm and lateral size of ∼300 nm is presented here by using a one-pot synthetic method. It is found that 1,10-phenanthroline plays an important role in determining the morphology of the SnSe product as three-dimensional SnSe nanoflowers are obtained in the absence of 1,10-phenanthroline while keeping other reaction parameters the same. The evolution process study discloses that single-crystalline nanosheets are obtained from the coalescence of the SnSe nucleus in an orientated attachment mechanism. Band gap determination and optoelectronic test based on hybrid films of SnSe and poly(3-hexylthiophene) indicate the great potential of the ultrathin SnSe nanosheets in photodector and photovoltaic, and so forth.

Since the first introduction of the strictly two-dimensional (2D) atomic crystal graphene, which represents many intriguing properties different from bulk graphite, it has sparked a diversity of applications.[1,2] More recently, some other types of 2D layered materials such as transition metal chalcogenides (TMCs) and transition metal oxides (TMOs) have also attracted tremendous attention due to their unique dimension-dependent properties.[3−7] By exfoliating the layered materials into 2D nanocrystals (NCs), novel electronic properties and high specific surface areas accompanying the enhancement of the host capabilities have been obtained and have been widely used in applications ranging from electronics to energy storage.[7,8] The past few years have witnessed great progress in producing the ultrathin materials.[7,9−12]

Among various 2D layered materials, the ultrathin TMCs have demonstrated unique electronic structures and physical properties compared with their bulk forms.[5,13−15] In particular, the colloidal IV-VI semiconductors have become one hot spot of recent research. As an important *p*-type IV-VI semiconductor, SnSe with a narrow band gap (∼0.90 eV indirect and ∼1.30 eV direct), which falls within the optimum band gap for solar cells (E_g = 1.0−1.5 eV), has attracted intense attention in solar cells research.[16−19] In addition, other advantages, such as earth-abundance, less toxicity, and chemical stability, have made the controlled synthesis and property study of SnSe a focus of interest.[16−18] It is well-known that SnSe adopts a layered crystal structure with atoms arranged resembling distorted NaCl structure. Similar to other group IV−VI binary semiconductor NCs such as SnS, GeS, and GeSe, the bonding of SnSe interacts covalently within the layer, which comprises zig-zag double layer planes of the tin and selenium atoms and is separated by a weak van der Waals force between the layers.[19−21] Benefiting from this, crystal growth along the [100] direction will prefer to the formation of orthorhombic SnSe with layered morphology. Although the synthesis of the SnSe NCs has been reported recently,[16−19,22] controlled synthesis of pure phase single-layer SnSe nanosheets (NSs) in a convenient way still remains a great challenge.

Herein, we present a one-pot colloidal route to prepare single-crystalline SnSe NSs with single-layer thickness. SeO_2 is used as the Se precursor[13,23,24] to replace the either expensive, air-sensitive, or high-toxic compounds such as bis-(trimethylsilyl)selenium and organophosphine selenide, as well as the selenium powder for its poor solubility in organic solvents.[16−18,25,26] To the best of our knowledge, this is the first instance for the synthesis of the single-layer single-crystalline SnSe NSs with four-atomic thickness. As a demonstration, the obtained SnSe NSs have been proven to show extraordinary photoresponse performance against previous reports.[17,18] We expect that the 2D confinement effect originating from the single-layer NS of SnSe will enable us to further investigate its undisclosed intrinsic physical properties, such as catalysis, anodic materials in lithium batteries, and so on.

In a typical reaction, a mixture of $SnCl_4{\cdot}5H_2O$ (0.1 mmol), SeO_2 (0.1 mmol), oleylamine (OAM, 10 mL), and 1,10-phenanthroline (Phen, 0.1 mmol) is added into a three-neck flask at room temperature, in which OAM acts as both reductant and capping ligand; and Phen functions as morphology control agent. After continuous stirring for 5 min, the reaction solution is degassed with high pure N_2 for 10 min at 120 °C, then heated up to 260 °C and aged for 30 min under N_2 atmosphere. Once the reaction is finished and cooled down to room temperature, the black products precipitated at the bottom of the flask are purified with excess ethanol by centrifugation and then are easily dispersed in apolar organic solvents (e.g., cyclohexane) for further characterization.

Figure 1A shows the typical transmission electron microscope (TEM) image of the SnSe NSs with lateral size of ∼300 nm. The thickness of the SnSe NSs is determined by atomic force microscope (AFM, Figure 1B). Surprisingly, the SnSe NSs possess a thickness of ∼1.0 nm, which is very close to the value of monolayer SnSe.[21,27] Statistical results of the sizes for the ultrathin SnSe NSs (including thickness and lateral size) by measuring 50 samples unambiguously confirm this observation (Figure S1). Additionally, some regular creases in the ultrathin SnSe NSs are observed under high resolution TEM (HR-TEM) with a neighboring distance of bumps around ∼2.8 nm, which

Received: November 2, 2012
Published: January 12, 2013

   dx.doi.org/10.1021/ja3108017 | *J. Am. Chem. Soc.* 2013, 135, 1213−1216

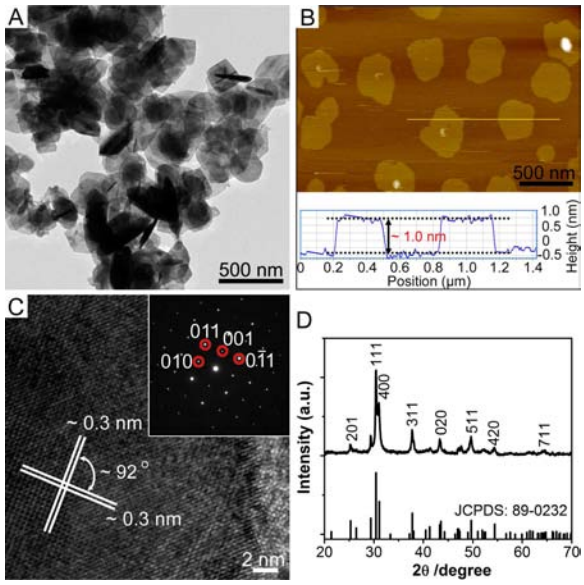

Figure 1. Characterizations of SnSe NSs. (A) TEM and (B) AFM images of SnSe NSs, with their height data. (C) HR-TEM image and SAED pattern of the SnSe NSs. (D) Powder XRD pattern of the SnSe NSs.

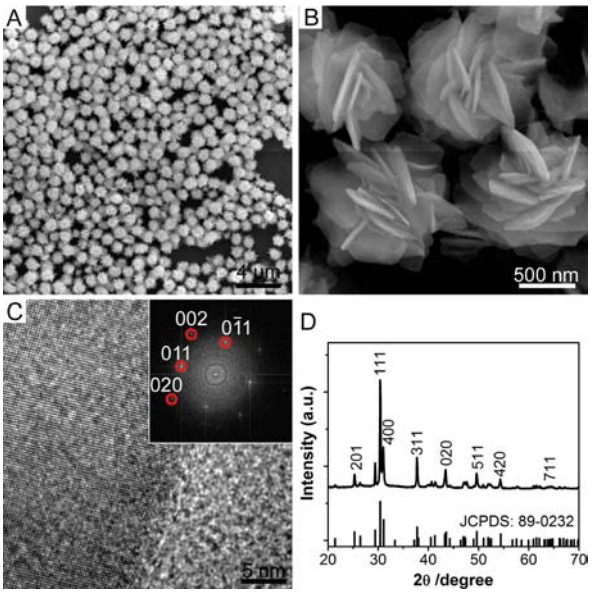

Figure 2. Characterizations of SnSe NFs. (A) SEM and (B) HR-SEM images of SnSe NFs. (C) HR-TEM image and SAED pattern (inset) of one petal from the SnSe NF. (D) Powder XRD pattern of the SnSe NFs.

is approximately 2 times the thickness of SnSe NSs in the presence of OAM (Figure S2). This evidence further illustrates the single-layer nature of the SnSe NSs. The single-crystalline feature of the SnSe NSs is verified by HR-TEM (Figure 1C). Two apparent planes revealing both lattice spacing at ∼0.3 nm and intersection angle of approximately 92° indicate the [011] plane sets of the SnSe NSs. In addition, the selected area electron diffraction pattern (SAED) of a single SnSe NS shows a spot pattern of *0kl* set reflection (inset in Figure 1C). These observations indicate that the SnSe NSs are normally orientated along [100] plane direction.[27,28]

Powder X-ray diffraction pattern (XRD) is performed to elucidate the phase structure of the SnSe NSs. As shown in Figure 1D, all of the diffraction peaks could be indexed to the orthorhombic SnSe with cell unit of a = 11.50 Å, b = 4.15 Å, and c = 4.45 Å (JCPDS No.89-0232, *Pnma*). It is worth noting here that, due to the formation of agglomerates and creases of the ultrathin SnSe NSs by van der Waals force (Figures 1A and S3), the XRD pattern of the SnSe NSs resembles that of bulk form.[24,29] The energy-dispersive spectroscopy (EDS) of the SnSe NSs depicts the molar ratio of Sn/Se as ∼0.95, which is well consistent with the stoichiometric ratio of the SnSe as 1:1 (Figure S4). This evidence unambiguously illustrates the pure phase of the as-obtained SnSe NSs.

Interestingly, if no Phen is added in the reaction system while keeping other parameters unchanged, 3D SnSe nanoflowers (NFs) are obtained. Figure 2A shows a typical scanning electron microscope (SEM) image of the SnSe NFs, displaying excellent monodispersity with 1.2 ± 0.2 μm in diameter. The high magnification SEM (Figure 2B) and TEM (Figure S5) images verify that the SnSe NFs are assembled from SnSe nanoplates. The HR-TEM image and SAED pattern of one petal in a SnSe NF proves the single-crystalline nature of the SnSe nanoplates, where the [100] orientation normal to the plane of SnSe nanoplates is also determined (Figure 2C). The XRD pattern of the SnSe NFs shows the same crystal structure as that of the SnSe NSs (Figure 2D). The EDS analysis further confirms an approximate 1:1 molar ratio of Sn/Se for SnSe NFs (∼0.92, Figure S6). It is notable that the obtained SnSe NSs and NFs are very rigid. A mild ultrasonication helps to disperse the SnSe NSs and NFs in solution for EM characterization, without destroying their structural integrity (Figure S7).

The growth mechanism is further investigated to disclose the origin of the two different morphologies of SnSe (NSs and NFs). Recently, Schaak and co-workers illustrated that the SnSe NSs could be produced in an oriented attachment mechanism, where single-crystalline NSs were obtained from the coalescence of initially formed SnSe NCs.[27] Here, we also propose that both the 2D SnSe NSs and 3D SnSe NFs experience the same process above. To verify this hypothesis, time-dependent growth of the SnSe NCs monitored by HR-TEM and SEM is performed. For SnSe NSs, in the early reaction stage, the initially formed SnSe NCs are found to quickly coalesce to form the poly-crystalline pseudo-sheets. Afterwards, these pseudo-sheets continue to grow up into single-crystalline NSs (Figure S8−S9), a phenomenon is similar to that of the PbS NSs formation.[12] As for SnSe NFs, the newly-formed poly-crystalline SnSe nanoplates could grow out both vertically and laterally, and then assemble into 3D NFs. Meanwhile, the ongoing ripening process under the guidance of surfactants OAM finally leads to the formation of single-crystalline SnSe NFs (Figures S10−S12).

On the basis of the above results, we conclude that Phen plays an important role in tuning the growth kinetics of SnSe since the only difference in preparing SnSe NSs and NFs is the addition of Phen. Phen is a classic bidentate chelate for transition metal ions because of its binitrogen atoms acting cooperatively in cation binding.[30] When Phen is mixed with OAM in the reaction for the synthesis of SnSe NSs, the Phen will strongly bind to the [100] lattice plane of the newly formed SnSe NCs in the early reaction stage, in cooperation with the adsorption of OAM on the [100] lattice plane.[30,31] The synergetic adsorption of Phen and OAM prohibits the subsequent growth along with [100] plane and keeps the thickness of SnSe NSs at a single layer scale. When no Phen is

dx.doi.org/10.1021/ja3108017 | *J. Am. Chem. Soc.* 2013, 135, 1213−1216

added, the complete suppression of the growth along [100] direction is partially relieved, which results in the lateral growth of the initial-formed SnSe NCs accompanying the mild growth along the vertical direction mediated by OAM, and finally leads to the formation of 3D SnSe NFs assembled from thicker SnSe nanoplates (Figures S11 and S12). To gain a deeper understanding of the interaction between SnSe NSs and Phen, X-ray photoelectron spectroscopy (XPS), Fourier transform infrared spectroscopy (FTIR) and UV−visible spectroscopy (UV−vis) have been employed in the study. Surprisingly, the results demonstrate that Phen is not anchored on the surfaces of the SnSe NSs and remains in the reaction solution after reaction (Figures S13−S15). Therefore, we hypothesize that Phen is dynamically absorbed/dissociated on the [100] plane of the newly formed SnSe NCs during the course of reaction, in cooperation with the adsorption of OAM onto the [100] plane (for more discussion, please see Supporting Information).[30,31] However, due to the lack of effective means to monitor this dynamic process *in situ*, it still remains a challenge for us to verify this hypothesis experimentally. Deeper understanding of the role of Phen will be executed in future work.

The diffuse reflectance spectroscopy is subsequently performed to acquire the band gaps of the SnSe NSs and SnSe NFs. As shown in Figure 3A, the onset absorption begins

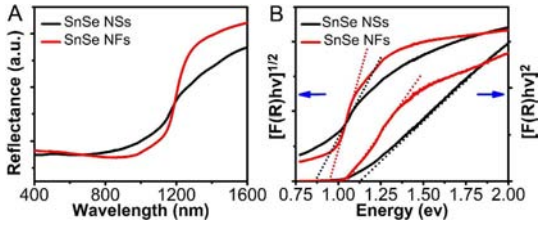

Figure 3. (A) Diffuse reflectance spectra of the SnSe NSs and NFs. (B) Determination of the band gaps by plotting $[F(R)h\nu]^{1/2}$ vs energy for indirect (left), and $[F(R)h\nu]^{2}$ vs energy for direct (right).

near 1300 nm for SnSe NSs and 1200 nm for SnSe NFs, respectively. By performing Kubelka−Munk transformation,[28,32] the indirect band gaps of the SnSe NSs and SnSe NFs are determined to be 0.86 and 0.95 eV, and the direct band gaps are 1.10 eV for SnSe NSs and 1.05 eV for SnSe NFs, respectively (Figure 3B). Both of the direct band gaps are red-shifted, while their indirect band gaps match very well with that of bulk SnSe.

The band structures of the two SnSe NCs are further investigated using the cyclic voltammetry (CV).[18] Figure 4A shows that the onset reduction potentials appear at −0.97 V for SnSe NSs and −0.91 V for SnSe NFs, respectively, which are both higher than that of the reported SnSe NCs.[17,18] Accordingly, the bottom of the conduction band (lowest unoccupied molecular orbital, LUMO) is determined to be −3.74 eV for SnSe NSs and −3.80 eV for SnSe NFs from the vacuum level. Besides, the top of the valence band (highest occupied molecular orbital, HOMO) values are also calculated to be −4.84 eV for SnSe NSs and −4.85 eV for SnSe NFs, by subtracting the direct band gaps, which are determined by diffuse reflectance in Figure 3B, from the LUMO values, respectively.

Since the band gaps of the two SnSe (NSs or NFs) fall within the major spectrum of the solar energy, their photoresponse properties are further investigated. Referring to a previous

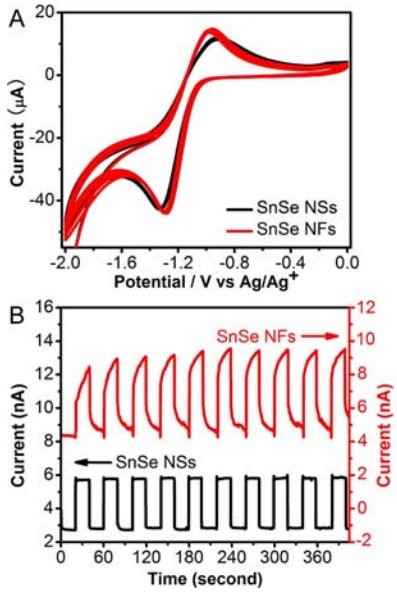

Figure 4. (A) CV of the SnSe NCs at a scan rate of 30 $mV{\cdot}s^{-1}$. (B) Transient photocurrent of the SnSe NCs films under illumination at an incident light density of 0.32 $mW{\cdot}cm^{-2}$ and an applied voltage of 2 V turned on and off at 20 s intervals.

literature,[25] a photodetector device comprising the SnSe NCs and poly-(3-hexylthiophene) (P3HT) hybrid films is constructed. As shown in Figure 4B, when the light is turned off, the measured dark currents at an applied voltage of 2 V are ∼2.8 nA for SnSe NSs and ∼4.8 nA for SnSe NFs, respectively. Upon turning on the light, a ∼2-fold enhancement of the photocurrent for both of the SnSe NSs and SnSe NFs is observed. By examing their response time, it is observed that the response time of SnSe NS-based hybrid photodetector is 0.19 s, whereas the response time of SnSe NF-based hybrid photodetector is 11.76 s (Figure S16). A similar trend of the current restored to their preillumination values of the SnSe NS- and SnSe NF-based hybrid photodetector is also observed, where the relaxation time of SnSe NFs is much longer than that of SnSe NSs (Figure S16). In addition, the optoelectronic performance of the pure P3HT is also evaluated under the same experimental condition (Figure S17). The results illustrate that the SnSe NCs dominate the photoresponse process in the inorganic−organic hybrid device under ON/OFF switching. Compared with previous reports of the photoresponse properties based on the SnSe NPs or nanowires,[17,18] much improved ON/OFF ratio and significantly shortened photoresponse time for the SnSe NSs are obtained here. Meanwhile, no apparent photocurrent degradation is observed up to 100 cycles. These observations suggest that the obtained single-layer single-crystalline SnSe NSs provide excellent charge dissociation and transportation benefitting from their ultrathin 2D characteristics. Furthermore, inspired by a recent work of Xue and co-workers,[20] which demonstrated a novel anisotropic ON/OFF switching property of a single micrometer-sized GeSe NS, further investigation on the anisotropic optoelectric properties of the single-layer SnSe NS is ongoing.

In summary, a facile, one-pot solution method has been explored to prepare ultrathin single-crystalline SnSe NSs with single-layer thickness of ∼1 nm in the presence of OAM and Phen. Phen is verified to play an important role in determining

dx.doi.org/10.1021/ja3108017 | *J. Am. Chem. Soc.* 2013, 135, 1213−1216

the morphology of SnSe NCs. Uniform 3D SnSe NFs are obtained without addition of Phen in the reaction. The evolution process studies disclose that the single-crystalline SnSe NSs are obtained from the coalescence of the SnSe nucleus in an orientated attachment mechanism. The band structures and their photoresponse properties of the SnSe NSs and SnSe NFs are comprehensively investigated, indicating their great potentials in optoelectric application. Considering the increasing interest in 2D NCs, we expect this convenient method may provide helpful guidance for preparing other ultrathin 2D NCs.

■ ASSOCIATED CONTENT

Supporting Information

Detailed experimental sections and characterizations. This material is available free of charge via the Internet at http://pubs.acs.org.

■ AUTHOR INFORMATION

Corresponding Author

qbwang2008@sinano.ac.cn

Notes

The authors declare no competing financial interest.

■ ACKNOWLEDGMENTS

We acknowledge funding by CAS "Bairen Ji Hua" program and "Strategic Priority Research Program" (Grant No. XDA 01030200), NSFC (Grant No. 21073225, 21101166) NSF of Jiangsu Province (Grant No. BK2012007), and the CAS/SAFEA International Partnership Program for Creative Research Teams.

■ REFERENCES

(1) Novoselov, K. S.; Jiang, D.; Schedin, F.; Booth, T. J.; Khotkevich, V. V.; Morozov, S. V.; Geim, A. K. *Proc. Natl. Acad. Sci. U.S.A.* **2005**, *102*, 10451.
(2) Novoselov, K. S.; Fal'ko, V. I.; Colombo, L.; Gellert, P. R.; Schwab, M. G.; Kim, K. *Nature* **2012**, *490*, 192.
(3) Ma, R.; Sasaki, T. *Adv. Mater.* **2010**, *22*, 5082.
(4) Radisavljevic, B.; Radenovic, A.; Brivio, J.; Giacometti, V.; Kis, A. *Nat. Nanotechnol.* **2011**, *6*, 147.
(5) Wang, M.-X.; Liu, C.; Xu, J.-P.; Yang, F.; Miao, L.; Yao, M.-Y.; Gao, C. L.; Shen, C.; Ma, X.; Chen, Xu, Z.-A.; Liu, Y.; Zhang, S.-C.; Qian, D.; Jia, J.-F.; Xue, Q.-K. *Science* **2012**, *336*, 52.
(6) Rogers, J. A.; Lagally, M. G.; Nuzzo, R. G. *Nature* **2011**, *477*, 45.
(7) Coleman, J. N.; Lotya, M.; O' Neill, A.; Bergin, S. D.; King, P. J.; Khan, U.; Young, K.; Gaucher, A.; De, S.; Smith, R. J.; Shvets, I. V.; Arora, S. K.; Stanton, G.; Kim, H.-Y.; Lee, K.; Kim, G. T.; Duesberg, G. S.; Hallam, T.; Boland, J. J.; Wang, J. J.; Donegan, J. F.; Grunlan, J. C.; Moriarty, G.; Shmeliov, A.; Nicholls, R. J.; Perkins, J. M.; Grieveson, E. M.; Theuwissen, K.; McComb, D. W.; Nellist, P. D.; Nicolosi, V. *Science* **2011**, *331*, 568.
(8) Seo, J.-w.; Jun, Y.-W.; Park, S.-W.; Nah, H.; Moon, T.; Park, B.; Kim, J.-G.; Kim, Y. J.; Cheon, J. *Angew. Chem.* **2007**, *119*, 8984.
(9) Son, J. S.; Yu, J. H.; Kwon, S. G.; Lee, J.; Joo, J.; Hyeon, T. *Adv. Mater.* **2011**, *23*, 3214.
(10) Huang, X.; Tang, S.; Mu, X.; Dai, Y.; Chen, G.; Zhou, Z.; Ruan, F.; Yang, Z.; Zheng, N. *Nat. Nanotechnol.* **2011**, *6*, 28.
(11) Yu, T.; Lim, B.; Xia, Y. *Angew. Chem., Int. Ed.* **2010**, *49*, 4484.
(12) Schliehe, C.; Juarez, B. H.; Pelletier, M.; Jander, S.; Greshnykh, D.; Nagel, M.; Meyer, A.; Foerster, S.; Kornowski, A.; Klinke, C.; Weller, H. *Science* **2010**, *329*, 550.
(13) Zhang, X.; Zhang, J.; Zhao, J.; Pan, B.; Kong, M.; Chen, J.; Xie, Y. *J. Am. Chem. Soc.* **2012**, *134*, 11908.
(14) Mak, K. F.; Lee, C.; Hone, J.; Shan, J.; Heinz, T. F. *Phys. Rev. Lett.* **2010**, *105*, 136805.
(15) Wang, Q. H.; Kalantar-Zadeh, K.; Kis, A.; Coleman, J. N.; Strano, M. S. *Nat. Nanotechnol.* **2012**, *7*, 699.
(16) Franzman, M. A.; Schlenker, C. W.; Thompson, M. E.; Brutchey, R. L. *J. Am. Chem. Soc.* **2010**, *132*, 4060.
(17) Baumgardner, W. J.; Choi, J. J.; Lim, Y.-F.; Hanrath, T. *J. Am. Chem. Soc.* **2010**, *132*, 9519.
(18) Liu, S.; Guo, X.; Li, M.; Zhang, W.-H.; Liu, X.; Li, C. *Angew. Chem., Int. Ed.* **2011**, *50*, 12050.
(19) Antunez, P. D.; Buckley, J. J.; Brutchey, R. L. *Nanoscale* **2011**, *3*, 2399.
(20) Xue, D.-J.; Tan, J.; Hu, J.-S.; Hu, W.; Guo, Y.-G.; Wan, L.-J. *Adv. Mater.* **2012**, *24*, 4528.
(21) Pejova, B.; Grozdanov, I. *Thin Solid Films* **2007**, *515*, 5203.
(22) Ning, J.; Xiao, G.; Jiang, T.; Wang, L.; Dai, Q.; Zou, B.; Liu, B.; Wei, Y.; Chen, G.; Zou, G. *CrystEngComm* **2011**, *13*, 4161.
(23) Chen, O.; Chen, X.; Yang, Y.; Lynch, J.; Wu, H.; Zhuang, J.; Cao, Y. C. *Angew. Chem., Int. Ed.* **2008**, *47*, 8638.
(24) Min, Y.; Moon, G. D.; Kim, B. S.; Lim, B.; Kim, J.-S.; Kang, C. Y.; Jeong, U. *J. Am. Chem. Soc.* **2012**, *134*, 2872.
(25) Wang, J.-J.; Wang, Y.-Q.; Cao, F.-F.; Guo, Y.-G.; Wan, L.-J. *J. Am. Chem. Soc.* **2010**, *132*, 12218.
(26) Allen, P. M.; Bawendi, M. G. *J. Am. Chem. Soc.* **2008**, *130*, 9240.
(27) II, D. D. V.; In, S.-I.; Schaak, R. E. *ACS Nano* **2011**, *5*, 8852.
(28) II, D. D. V.; Patel, R. J.; Hickner, M. A.; Schaak, R. E. *J. Am. Chem. Soc.* **2010**, *132*, 15170.
(29) Li, D.; Müller, M. B.; Gije, S.; Kaner, R. B.; Wallace, G. G. *Nat. Nanotechnol.* **2008**, *3*, 101.
(30) Mirkovic, T.; Hines, M. A.; Nair, P. S.; Scholes, G. D. *Chem. Mater.* **2005**, *17*, 3451.
(31) Zhang, Y.; Lu, J.; Shen, S.; Xu, H.; Wang, Q. *Chem. Commun.* **2011**, *47*, 5226.
(32) Hagfeldt, A.; Graetzel, M. *Chem. Rev.* **1995**, *95*, 49.